



Cathepsin K cleavage of SDF-1 α inhibits its chemotactic activity towards glioblastoma stem-like cells



Vashendriya V.V. Hira^{a,b,*}, Urška Verbovšek^{c,1}, Barbara Breznik^{c,d}, Matic Srdič^e, Marko Novinec^e, Hala Kakar^a, Jill Wormer^a, Britt Van der Swaan^a, Brigita Lenarčič^e, Luiz Juliano^f, Shwetal Mehta^b, Cornelis J.F. Van Noorden^a, Tamara T. Lah^{c,d,e}

^a Department of Cell Biology and Histology, Academic Medical Center, University of Amsterdam, Meibergdreef 15, 1105 AZ Amsterdam, The Netherlands

^b Division of Neurobiology, Barrow Brain Tumor Research Center, Barrow Neurological Institute, St. Joseph's Hospital and Medical Center, Phoenix, AZ 85013, USA

^c Department of Genetic Toxicology and Cancer Biology, National Institute of Biology, Večna pot 111, 1000 Ljubljana, Slovenia

^d Jozef Stefan International Postgraduate School, Jamova 39, 1000 Ljubljana, Slovenia

^e Department of Biochemistry, Faculty of Chemistry and Chemical Engineering, University of Ljubljana, Večna pot 113, 1000 Ljubljana, Slovenia

^f Department of Biophysics, Medical School, Federal University of Sao Paulo, Brazil

ARTICLE INFO

Article history:

Received 12 August 2016

Received in revised form 22 December 2016

Accepted 27 December 2016

Available online 28 December 2016

Keywords:

Glioma stem-like cells

Niche

Stromal-derived factor-1 α

Cathepsin K

ABSTRACT

Glioblastoma (GBM) is the most aggressive primary brain tumor with poor patient survival that is at least partly caused by malignant and therapy-resistant glioma stem-like cells (GSLCs) that are protected in GSLC niches. Previously, we have shown that the chemo-attractant stromal-derived factor-1 α (SDF-1 α), its C-X-C receptor type 4 (CXCR4) and the cysteine protease cathepsin K (CatK) are localized in GSLC niches in glioblastoma. Here, we investigated whether SDF-1 α is a niche factor that through its interactions with CXCR4 and/or its second receptor CXCR7 on GSLCs facilitates their homing to niches. Furthermore, we aimed to prove that SDF-1 α cleavage by CatK inactivates SDF-1 α and inhibits the invasion of GSLCs. We performed mass spectrometric analysis of cleavage products of SDF-1 α after proteolysis by CatK. We demonstrated that CatK cleaves SDF-1 α at 3 sites in the N-terminus, which is the region of SDF-1 α that binds to its receptors. Confocal imaging of human GBM tissue sections confirmed co-localization of SDF-1 α and CatK in GSLC niches. In accordance, 2D and 3D invasion experiments using CXCR4/CXCR7-expressing GSLCs and GBM cells showed that SDF-1 α had chemotactic activity whereas CatK cleavage products of SDF-1 α did not. Besides, CXCR4 inhibitor plerixafor inhibited invasion of CXCR4/CXCR7-expressing GSLCs.

In conclusion, CatK can cleave and inactivate SDF-1 α . This implies that CatK activity facilitates migration of GSLCs out of niches. We propose that activation of CatK may be a promising strategy to prevent homing of GSLCs in niches and thus render these cells sensitive to chemotherapy and radiation.

© 2016 Elsevier B.V. All rights reserved.

1. Introduction

Glioblastoma (GBM) is the most malignant primary brain tumor with poor patient survival despite surgery, irradiation and chemotherapy. This is at least partly due to the existence of glioma stem-like cells (GSLCs) that are resistant to therapy [1–6]. Therefore, targeting GSLCs is the key to improve anti-GBM therapy [1–6]. GSLCs reside in protective niches, which are at least partly responsible for their resistance to

therapy [1,7,8]. We have shown in a previous study in human GBM that GSLCs reside around the endothelium of arterioles in hypoxic niches, expressing the chemokine stromal-derived factor-1 α (SDF-1 α), its receptors C-X-C receptor type 4 (CXCR4) and the cysteine protease cathepsin K (CatK) [9]. These proteins are also functional in hematopoietic stem cell (HSC) niches in human bone marrow, where CXCR4-positive HSCs are retained in hypoxic niches by high levels of SDF-1 α [10–13] (Hira et al., submitted). Bone-resorbing osteoclasts in bone marrow release several proteases during stress conditions, such as CatK that alone or collectively inactivate SDF-1 α , resulting in migration of HSCs out of HSC niches into the circulation [12,14,15] (Hira et al., submitted).

The SDF-1 α /CXCR4 signaling axis is overexpressed in many types of cancer, including GBM [7,16,17]. Another receptor for SDF-1 α is CXCR7 that is like CXCR4 overexpressed in GBM cells and in particular in GSLCs [18–21]. This upregulation of SDF-1 α , CXCR4 and CXCR7 in GBM is

Abbreviations: CatK, cathepsin K; CXCR4/7, C-X-C receptor type 4/7; GBM, glioblastoma; GSLC, glioma stem-like cell; HIF-1 α , hypoxia-inducible factor-1 α ; HSC, hematopoietic stem cell; IHC, immunohistochemistry; SDF-1 α , stromal-derived factor-1 α ; VEGF, vascular endothelial growth factor.

* Corresponding author at: Academic Medical Center, Department of Cell Biology and Histology, Meibergdreef 15, 1105 AZ Amsterdam, The Netherlands.

E-mail address: v.v.hira@amc.uva.nl (V.V.V. Hira).

¹ Authors contributed equally.

induced by hypoxia-inducible factor-1 α (HIF-1 α) and vascular endothelial growth factor (VEGF) [16,17], which are abundantly expressed in and around GSLC niches [9]. GSLCs are attracted by SDF-1 α [22–27] and the SDF-1 α /CXCR4 and SDF-1 α /CXCR7 axes can facilitate homing of GSLCs into GSLC niches and protect GSLCs against chemo-irradiation [7]. Therefore, the development of novel strategies is in progress to prevent homing of GSLCs in niches and/or to enforce migration of GSLCs out of niches to render these cells sensitive to chemo-irradiation [7,8] (Hira et al., submitted).

CatK is an endolysosomal cysteine endopeptidase and is one of the highest differentially expressed proteases in GBM as compared to normal brain [28,29]. This was shown in an *in silico* study of gene expression in human GBM using publically-available data sets, in GBM tissue samples and in GBM cell lines. The overexpression of CatK was validated with RT-PCR, western blotting and immunohistochemistry [29]. However, activity of CatK has not been detected in extracts of GBM tissues and cells, in contrast to the high activity of CatB and CatS that is likely involved in invasion [30]. CatK activity may well not be detected because it is tightly regulated, which is needed to control its highly destructive proteolytic power [28,29,31]. Since CatK can cleave SDF-1 α in human HSC niches [12,14,15] (Hira et al., submitted) and it is expressed in GSLC niches together with SDF-1 α [9,28], we hypothesize that SDF-1 α facilitates homing of CXCR4 and/or CXCR7-positive GSLCs in niches and that CatK regulates SDF-1 α activity [9]. In the present study, we provide supporting evidence for this concept.

2. Materials and methods

2.1. Cell culture

NCH421k GSLCs [32,33] were a generous gift from Prof. Christel Herold-Mende (Heidelberg University, Heidelberg, Germany), and were cultured in Neurobasal medium (Gibco Life Technologies,

Carlsbad, CA, USA) containing 1% penicillin/streptomycin (Sigma, St. Louis, MO, USA), 1% L-glutamine (Sigma), 2% B27, 0.08% bFGF (Gibco), 0.01% EGF (Gibco) and 0.01% heparin (Sigma) at 37 °C in a 5% CO₂ incubator. U87 GBM cells (ATCC, Teddington, Middlesex, UK) were cultured in DMEM medium (Sigma) containing 1% penicillin/streptomycin, 1% L-glutamine and 10% fetal bovine serum (Gibco) at 37 °C in a 5% CO₂ incubator. These cells were authenticated as described by Torsvik et al. [34]. Patient-derived cell line GB7 was established from resected primary GBM tumor tissue at the Barrow Neurological Institute, Phoenix, AZ, USA. These GSLCs were grown as neurospheres (Gibco) in DMEM and F12-Glutamax (Gibco) supplemented with B27 (Thermo Fisher Scientific; Waltham, MA, USA) and N2 (Thermo Fisher Scientific) in the presence of 20 ng/mL EGF (EMD Millipore; Billerica, MA, USA) and 20 ng/mL bFGF (EMD Millipore).

2.2. Quantitative real-time PCR

Quantitative real-time PCR (qRT-PCR) was performed to assess mRNA levels of CXCR4 and CXCR7. Total RNA was isolated from NCH421k and U87 cells using Trizol reagent (Invitrogen). cDNA was generated from 1 μ g total RNA using a High Capacity cDNA Reverse Transcription Kit (Applied Biosystems; Carlsbad, CA, USA). Real-time PCR was performed with the ABI 7900 HT Sequence Detection System (Applied Biosystems) using Taqman gene expression assays (Applied Biosystems) for the detection of CXCR4 and CXCR7 mRNA expression. Glyceraldehyde 3-phosphate dehydrogenase (GAPDH) was used as internal control. The primers Hs00607978_s1 (Applied Biosystems), Hs00604567_m1 (Applied Biosystems) and No. 4310884E (Applied Biosystems) were used for CXCR4, CXCR7 and GAPDH, respectively. Analyses were performed with SDS v2.2 software (Applied Biosystems). The experiments were performed in triplicate.

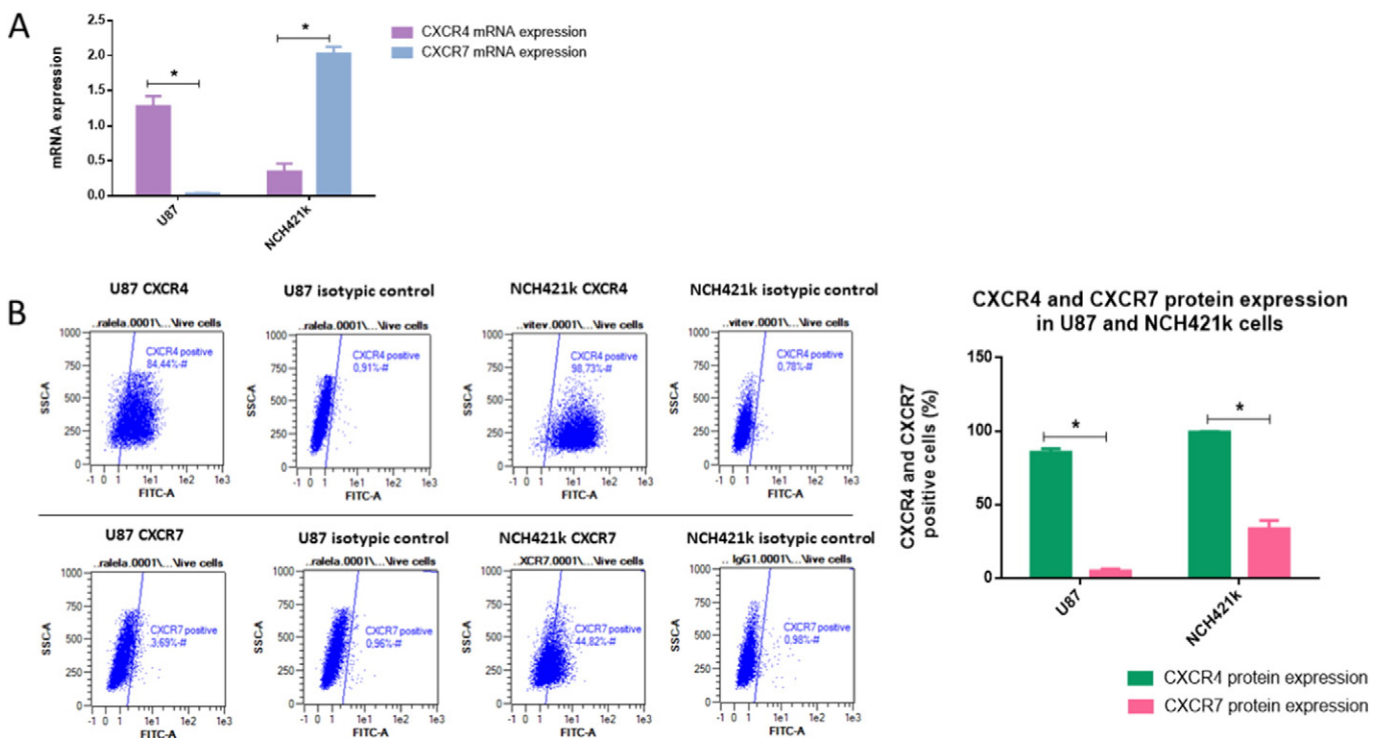


Fig. 1. mRNA and protein expression of CXCR4 and CXCR7 in U87 and NCH421k cells. (A) q-RT-PCR analysis of lysates of NCH421k GSLCs and U87 GBM cells was performed to determine their CXCR4 and/or CXCR7 mRNA expression. NCH421k GSLCs had a relatively low expression of CXCR4 and a high expression of CXCR7. U87 GBM cells had a relatively high expression of CXCR4 and virtually no expression of CXCR7. (B) Flow cytometry analysis was performed to determine CXCR4 and CXCR7 protein expression on U87 and NCH421k cells. The CXCR4 protein levels were equally high on both cell lines, whereas CXCR7 protein expression was higher on NCH421k cells as compared to U87 cells. The error bars represent the standard error of the mean. *, $P < 0.05$.

2.3. Flow cytometry analysis

Flow cytometry analysis was performed to determine CXCR4 and CXCR7 expression on the cell surface of NCH421k and U87 cells. One million NCH421k and U87 cells were harvested and washed twice in buffer (2% BSA in 1× PBS). Cells were incubated with primary antibodies against CXCR4 (1:500, R&D Systems, MAB42273; Minneapolis, MI, USA) and CXCR7 (1:50; R&D Systems, MAB172) for 30 min at 4 °C. After a washing step with buffer, cells were incubated with secondary antibody rabbit anti-mouse Alexa Fluor 488 (Life Technologies, Carlsbad, CA, USA) for 30 min at 4 °C, followed by another washing step with buffer and resuspension in 1× PBS. Propidium iodide (1:100, Miltenyi Biotec; San Diego, CA, USA) was added to the cell suspensions to exclude dead cells. Analysis was performed using the flow cytometer MACSQuantify Analyzer 10 (Miltenyi Biotec) and MACSQuantify software (Miltenyi Biotec). Protein expression was observed in the FITC channel and isotopic controls (IgG2B and IgG1, Abcam) were used in the same concentrations as the primary antibodies to control for aspecific background staining.

2.4. Western blot analysis

Whole-cell lysates of GSLC line GB7 were generated using standard RIPA buffer (20 mM HEPES at pH 8.0, 1% NP40, 0.5% sodium deoxycholate, 0.1% SDS, 25 mM EDTA) containing complete phosphatase and protease inhibitors (Thermo Fisher Scientific), rotated at 4 °C for 30 min and then centrifuged at maximum speed to collect the supernatant. Protein concentrations were determined using the Bradford Assay (Thermo Fisher Scientific) and equal amounts of protein (30 µg) were loaded and transferred to PVDF membranes (EMD Millipore). Membranes were blocked in 5% BSA in TBST (Tris-buffered saline, 0.1% Tween 20) buffer for 1 h at RT, and incubated overnight with primary antibodies at 4 °C. Western blots were processed with fluorescent secondary antibodies (Pierce Dylight, ThermoFisher Scientific) and developed with ClxLiCor Odyssey (Li-Cor; Lincoln, NE, USA). The following antibodies were used for western blotting: rabbit anti-human CXCR4 (Abcam, Cambridge, UK), rabbit anti-human CXCR7 (Santa Cruz Biotechnologies) and mouse anti-human vinculin (Abcam) as loading control.

2.5. Proteolytic processing of SDF-1 α by CatK

Proteolytic cleavage of SDF-1 α by CatK was performed *in vitro* to determine the cleavage sites of SDF-1 α (Peptide, Rocky Hill, NJ, USA) generated by CatK. Recombinant human procathepsin K was prepared as described previously [35]. Purified procathepsin K was activated *in vitro* at pH 4.0 and 37 °C. CatK activity was stopped by adjusting the pH of the activation mixture to ~5.5. The active enzyme concentration was determined by active site titration using the irreversible cysteine cathepsin inhibitor E-64 (Bachem, Bubendorf, Switzerland). Hydrolysis was performed in 100 mM sodium acetate buffer pH 5.5 or in 50 mM HEPES buffer pH 7.4, each buffer containing 1 mM EDTA and 5 mM dithiothreitol (DTT). Reaction mixtures containing 20 µM SDF-1 α and 0.4 µM CatK were incubated on a Thermomixer (Eppendorf, Hamburg, Germany) at 37 °C. The pH 5.5 reaction mixture was incubated for 30 min and the pH 7.4 reaction mixture was incubated for 15 min. Reactions were stopped either by the addition of E-64 in an amount equimolar to the CatK concentration or, alternatively, by selective removal of the produced small fragments by filtration through a 0.5 mL Ultra centrifugal filter (Amicon, Temecula, CA, USA) with a 3 kDa cut-off at 4 °C. The complete reaction mixtures, as well as mixtures of short cleavage products only, were used in further experiments. To determine the size and identity of the cleavage products, peptides generated by CatK were analyzed at the commercial proteomics facility at the Jožef Stefan Institute using matrix-assisted laser desorption/ionization time-of-flight (MALDI-TOF) mass spectrometry (Bruker, Bremen, Germany).

2.6. Two-dimensional invasion assays

Invasion assays were performed using the transwell chambers, inserts with 8.0 µm pores (Corning, Life Sciences, New York, NY, USA) and 2 cell lines: U87 cells (40,000 cells/insert) and NCH421k cells (80,000 cells/insert). The inserts were coated with 0.5 mg/mL Matrigel (Corning) and dried overnight. Cells were plated in serum-free medium in the upper chamber and normal medium containing SDF-1 α or its derivatives were placed in the lower chamber: (1) SDF-1 α (10 ng/mL); (2) PepC-C (3 ng/mL; sequence of 21 amino acids from the N-terminal end of SDF-1 α , KPVLSYRCPCRFESHVARANVKHLKILN, as described in [36]); (3) complete reaction mixture at pH 5.5 (10 ng/mL); (4) complete reaction mixture at pH 7.4 (10 ng/mL); (5) and (6) complete cleavage products of SDF-1 α at pH 5.5 and 7.4 (10 ng/mL), respectively; (7) and (8) synthetic copies of peptides (10 ng/mL; KPVS and KPVSLS, respectively; GenicBio, Shanghai, China) that are cleavage products of SDF-1 α generated by CatK, and (9) medium only as a control. After 48 h of incubation at 37 °C, tetrazolium salt MTT (Sigma) was added to the upper and lower chambers and

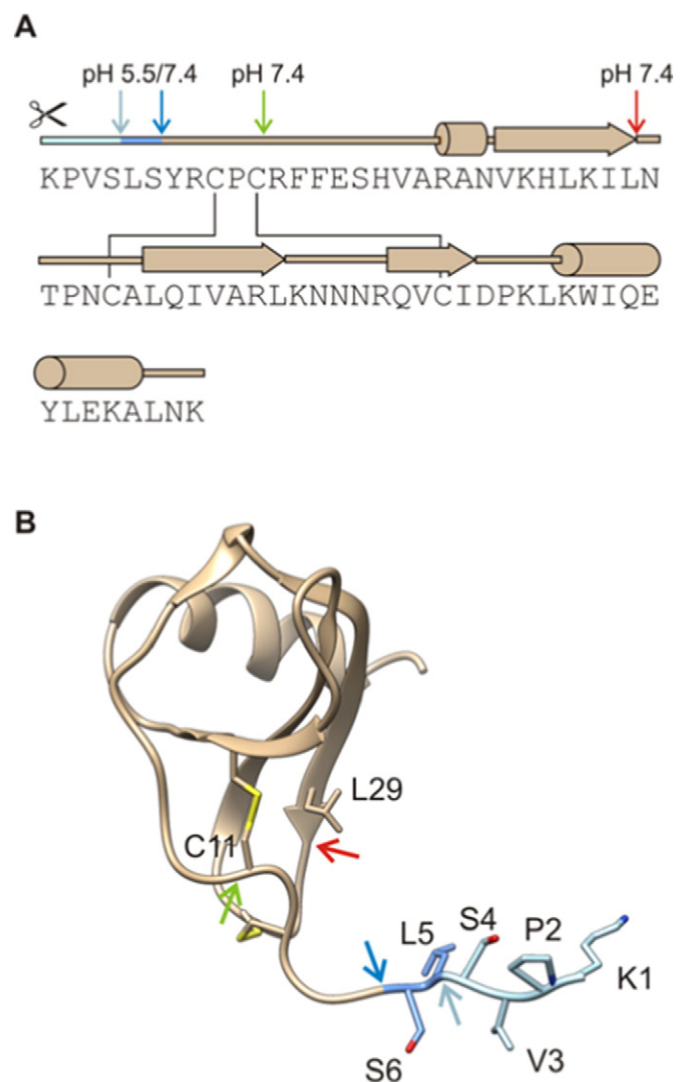


Fig. 2. CatK-induced cleavage products of SDF-1 α . (A) Amino acid sequence of SDF-1 α and the cleavage sites by CatK at pH 5.5 and/or pH 7.4. Cleavage sites are indicated by arrows and the secondary structure elements are shown above the amino acid sequence. (B) Three-dimensional (3D) molecular structure of SDF-1 α with cleavage sites mapped onto the 3D structure of SDF-1 α (PDB accession code 2N55). Residue numbering applies to the mature form of SDF-1 α . The 2 disulfide bonds, the N-terminal 6 residues and Leu29 of SDF-1 α are shown as sticks. The image was created with UCSF Chimera—a visualization system for exploratory research and analysis as described in [44]).

the incubation at 37 °C lasted for another 3 h. Then, formazan crystals were collected separately from each chamber, pelleted by centrifugation, dissolved in dimethylsulfoxide (DMSO) and the absorbance at 570 and 690 nm was measured using a plate reader (Synergy Mx, BioTek, Winooski, VT, USA). The relative invasion (%) was determined as the ratio of absorbance in the lower chamber and the sum of absorbance in both chambers. The experiments were performed in triplicate.

2.7. Three-dimensional invasion assays

NCH421k cells were seeded in complete Neurobasal medium (Gibco) containing 4% methylcellulose in U-bottomed 96-well plates with 3000 cells/well (BD Biosciences, San Diego, CA, USA) centrifuged at $850 \times g$ and 31 °C for 90 min and incubated at 37 °C in a 5% CO₂ incubator for 3 days to form one spheroid in each well. Spheroids were transferred into 24-well plates (Corning) and embedded in 6.0 mg/mL Matrigel (Corning). After 30 min of incubation at 37 °C in a 5% CO₂ incubator, spheroids were covered with complete Neurobasal medium containing SDF- α (10 ng/mL), PepC-C (3 ng/mL) and cleavage products of SDF-1 α generated by CatK at pH 5.5 or pH 7.4 (10 ng/mL; after filtration and removal of peptides >3 kDa). As a control, only complete Neurobasal medium was used to cover the spheroids. Numbers of GSLCs that invaded from the spheroids into the Matrigel were determined using image analysis after day 3 and day 6 using an inverted fluorescence microscope (Nikon Eclipse Ti, Tokyo, Japan) at 4 \times magnification and NIS-Elements, Nikon software [37].

2.8. Cell viability assay

Fifty thousand GB7 cells were seeded on 6-well plates and were treated with 10, 25, 50, 100 and 500 nM of the CXCR4 inhibitor plerixafor (Selleck; Houston, TX, USA) for 24 h at 37 °C in a 5% CO₂ incubator. The number of viable cells was determined using a trypan blue exclusion assay to assess the toxicity of plerixafor.

2.9. Plerixafor-treated GSLCs in transwell invasion assays

The effect of plerixafor on invasion of GB7 GSLCs was determined using transwell assays and collagen-coated (Advanced BioMatrix; San Diego, CA, USA) inserts with a pore size of 8 μ m (Becton Dickinson;

Franklin Lakes, NJ, USA). Dissociated GB7 cells (50,000/insert) were re-suspended in serum-free media with growth factors (20 ng/mL EGF and bFGF) and mixed with thawed Matrigel (BD Biosciences; San Jose, CA, USA). A total of 50 μ L of Matrigel plus cell suspension was placed on the inserts in duplicates. Inserts were then placed in 24-well plates. After 24 h, invaded GB7 cells that accumulated on the bottom surface of the insert membrane were fixed with 4% paraformaldehyde for 20 min, washed with $1 \times$ PBS for 10 min and stained with DAPI (1:1000 in $1 \times$ PBS) for 10 min. The membranes were subsequently cut out and mounted on microscopic slides for quantification. Images of the membranes were taken using the fluorescence microscope (Zeiss; Jena, Germany) and the ZenPro software (Zeiss). The total number of cells in five individual fields per membrane was counted using Image J software [37,38]. Cells treated with 10, 25, 50, 100 and 500 nM plerixafor were compared with the control and in all transwells, SDF-1 α (10 ng/mL) was used as chemo-attractant.

2.10. Brain tumor samples of patients

GBM samples from 10 patients were obtained from the Brain Tumor Bank maintained by the Department of Neuropathology at the Academic Medical Centre (AMC, Amsterdam, The Netherlands). Research was performed on “waste” material that was stored in a coded fashion. Consent for this project was reviewed and waived, and the project was approved by the Medical Ethics Review Committee of the Academic Medical Center and University of Amsterdam (reference number W14_224 # 14.17.0286). Consent for removal of the tissue and its storage in the tumor bank for research purposes was obtained and documented in the patients' medical charts. Tissue samples were snap-frozen in liquid nitrogen in the operating room and stored at -80 °C until use. Cryostat sections (7- μ m thick) were cut at -25 °C on an HM560 cryostat (MICROM, Walldorf, Germany), picked up on glass slides, and stored at -80 °C until use. All staining procedures, including those for controls, were performed on serial sections of each GBM sample [9].

2.11. Chromogenic immunohistochemistry

Immunohistochemistry (IHC) was performed on serial GBM cryostat sections. Sections were air-dried at room temp for 15 min before

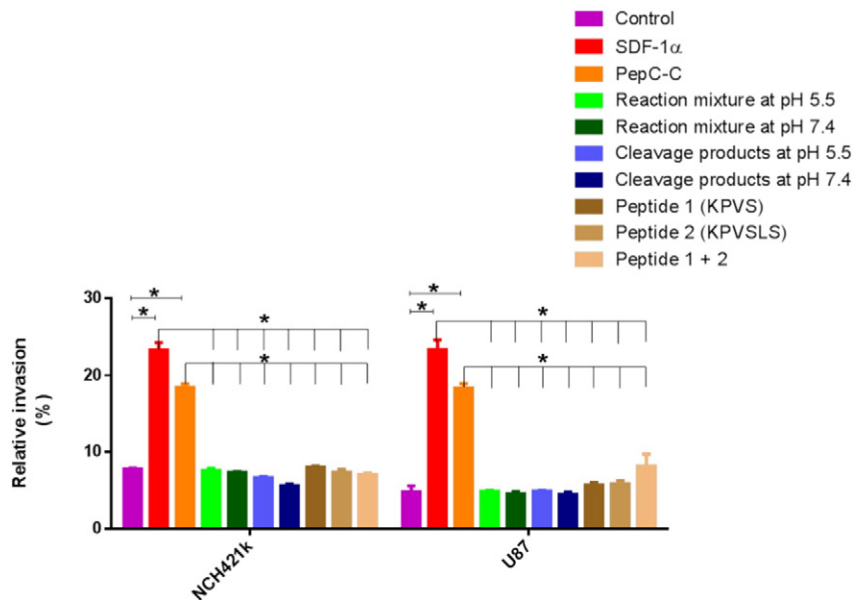


Fig. 3. Transwell invasion assays of NCH421k GSLCs and U87 GBM cells. Relative cell invasion percentages from the upper chamber to the lower chamber were determined after 48 h of incubation in transwells. The data shows that SDF-1 α and PepC-C had a strong chemotactic effect on NCH421k GSLCs and U87 GBM cells as compared to control, complete reaction mixtures after incubation of SDF-1 α and CatK and small cleavage products only after filtration (<3 kDa). The two small synthetic peptides (KPVS and KPVLS) did not show any chemotactic effects in both cell lines either. The error bars represent the standard error of the mean. *, $P < 0.05$.

staining. Sections were fixed in acetone ($-20\text{ }^{\circ}\text{C}$) for 10 min and air-dried afterwards for 15 min. Sections were encircled with a PAP pen (Dako, Glostrup, Denmark), followed by 3 washing steps of 5 min with PBS. The sections were treated with 100% methanol containing 0.3% H_2O_2 for 15 min to block endogenous peroxidase activity and to prevent non-specific background staining, followed by 3 washing steps of 5 min each using PBS. Then, sections were incubated with PBS containing 10% normal goat serum (Dako) and 0.1% bovine serum albumin (BSA) for 45 min to further reduce nonspecific background staining. After tapping off the goat serum-containing buffer, sections were incubated overnight at $4\text{ }^{\circ}\text{C}$ with primary antibodies (rabbit-anti-human CatK, ab19027, dilution 1:200, Abcam, Cambridge, UK; rabbit-anti-human SDF-1 α , MAB310, dilution 1:200, R&D Systems; mouse-anti-human smooth muscle actin (SMA), M0851 clone 1A4, dilution 1:500, Dako). After incubation with primary antibodies, sections were washed 3 times for 5 min in PBS containing 0.1% BSA. Sections incubated with

antibodies against CatK and SDF-1 α were incubated with polyclonal goat-anti-rabbit secondary antibody conjugated with horse-radish peroxidase (HRP) (Dako) in a 1:200 dilution in PBS containing 0.1% BSA for 1 h. Sections incubated with antibodies against SMA were incubated with polyclonal goat-anti-mouse secondary antibody conjugated with HRP (Dako) in a 1:200 dilution in PBS containing 0.1% BSA for 1 h. Incubation with secondary antibodies was followed by 3 washing steps of 5 min with PBS. After that, sections were incubated with AEC (peroxidase substrate kit; Vector Laboratories, Burlington, CA, USA) for 20 min, followed by one washing step of 5 min using PBS. Sections were placed in running tap water for 20 min and then in distilled water followed by incubation for 3 min in hematoxylin (Fluka Biochemica, Sigma-Aldrich) for nuclear staining. Sections were again placed in running tap water for 20 min and then in distilled water. All incubation steps were performed at room temp, except for the overnight incubations with primary antibodies that were performed at

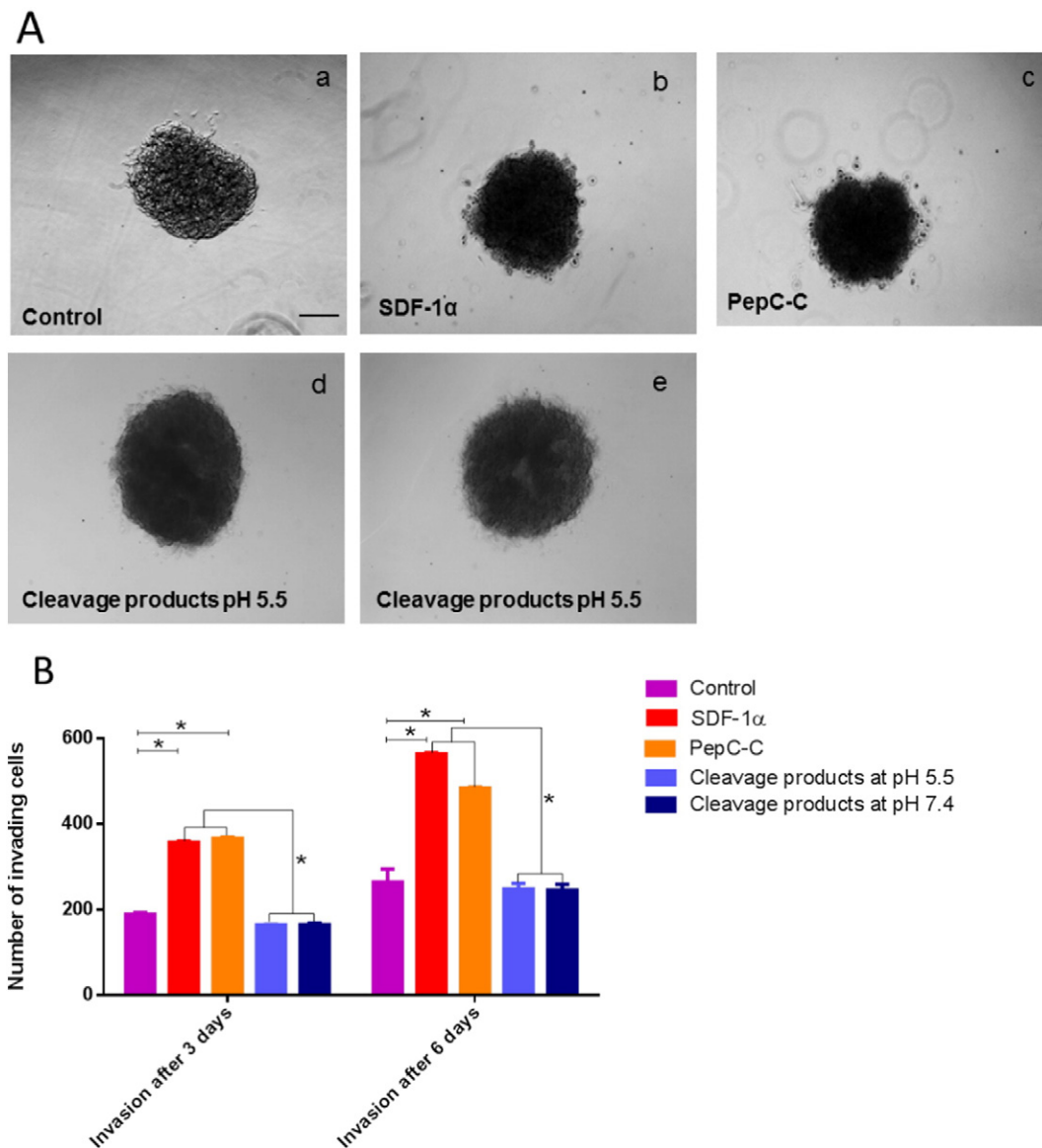


Fig. 4. Spheroid invasion assays using NCH421k GSLCs. (A) Images of spheroids surrounded by invading NCH421k GSLCs. Spheroids embedded in Matrigel were incubated for 6 days in the presence of SDF-1 α (b), PepC-C (c), cleavage products of SDF-1 α generated by CatK at pH 5.5 (d), cleavage products of SDF-1 α generated by CatK at pH 7.4 (e) and control with medium only (a). Scale bar = 100 μm . Please note that images were captured of spheroids in the center and invading cells in the vicinity of the spheroids. However, cells invaded over larger distances away from the spheroids. (B) Numbers of GSLCs invading into Matrigel out of spheroids were determined using image analysis after treatment with SDF-1 α , PepC-C, cleavage products of SDF-1 α generated by CatK at pH 5.5 and 7.4 (<3 kDa) and medium only as control. All invaded cells, including the cells that invaded over larger distances than shown in Fig. 4A have been quantified. The data shows that treatment with SDF-1 α and PepC-C significantly increased the numbers of GSLCs invading into the Matrigel out of spheroids as compared to the control and cleavage products of SDF-1 α <3 kDa generated by CatK. The error bars represent the standard error of the mean. *, $P < 0.05$.

4 °C. Finally, sections were covered with glycerin/gelatin mounting medium (Sigma-Aldrich). Control incubations were performed in the absence of primary antibody. The second control panel was performed with rabbit serum or mouse serum in the same concentration as the primary antibody, to determine the effect of the serum on non-specific background staining.

2.12. Fluorescence immunohistochemistry

Sections were air-dried for 30 min at room temp, encircled using a PAP-pen (Daido Sangyo, Tokyo, Japan) and fixed for 10 min at room temp by using 4% paraformaldehyde (Acros Organics, Geel, Belgium) containing 3.7% methanol (Merck, Darmstadt, Germany) diluted in PBS. Sections were washed twice in PBS, followed by permeabilization using 0.1% Triton X (Sigma) in PBS and 2 washing steps in PBS. Blocking of non-specific staining was performed by incubation in PBS containing 0.5% BSA (Sigma). Afterwards, sections were incubated with primary antibodies at room temp (rabbit-anti-human CatK (isotype IgG), ab19027, dilution 1:500, Abcam; mouse-anti-human SDF-1 α (isotype IgG1), MAB310, dilution 1:600, R&D Systems; rabbit-anti-human SMA, (isotype IgG2a), M0851 clone 1A4, dilution 1:500, Dako). Single, double or triple staining procedures were used for the 3 primary antibodies. After 60 min of incubation at room temp, sections were washed with PBS. Incubation with secondary antibodies was performed for 30 min at room temp (goat-anti-rabbit CatK (IgG) conjugated with Alexa 488, dilution 1:500, Invitrogen, Carlsbad, CA, USA; goat-anti-mouse SDF-1 α (IgG1) conjugated with Alexa 647, dilution 1:500, Life Technologies, Carlsbad, CA, USA; goat-anti-mouse SMA (IgG2a) conjugated with Alexa 568, dilution 1:500, Life Technologies). Removal of fluorescent lipofuscin from sections was performed by incubation for 30 min in 30 mM ammonium acetate (Merck, Darmstadt, Germany), and 10 mM copper sulphate (Merck). Afterwards, sections were washed for 30 s using distilled water and 4 times 5 min using PBS. Sections were mounted in ProLong Gold containing DAPI (Life Technologies, Bleiswijk, The Netherlands) and coverslipped. Preparations were hardened overnight at room temp. Control incubations were performed in the absence of primary antibodies. Imaging was performed using a confocal

microscope (SP8-X SMD; Leica, Amsterdam, The Netherlands). Images of 1024 \times 1024 pixels were taken as optical sections and were analyzed using LAS X software (Amsterdam, The Netherlands).

2.13. Statistical analyses

Data were processed in Excel 2013 (Microsoft, Redmond, WA, USA) and GraphPad Prism 6 (La Jolla, CA, USA) for statistical analyses using *t*-tests for qRT-PCR data and one-way ANOVA tests for invasion assays. *P* values <0.05 were considered to indicate significant differences.

3. Results

3.1. Cellular expression of CXCR4 and CXCR7

Fig. 1A shows CXCR4 and CXCR7 mRNA expression levels in NCH421k GSLCs and U87 GBM cells. NCH421k cells had a relatively low expression of CXCR4 and a high expression of CXCR7, whereas U87 cells had a relatively high expression of CXCR4 and virtually no expression of CXCR7. However, flow cytometry analysis revealed that both U87 and NCH421k cells had a high and similar level of CXCR4 protein expression on the cell surface, whereas CXCR7 protein expression was higher on NCH421k cells as compared to U87 cells (Fig. 1B).

3.2. Proteolytic processing of SDF-1 α by CatK

It has been shown in previous studies that CatK and other cysteine cathepsins can cleave SDF-1 α [39]. To determine the effect of the CatK-induced cleavage on the chemotactic activity of SDF-1 α , we analyzed the cleavage of SDF-1 α in more detail, as presented in Fig. 2A. Since CatK is active in both the endolysosomal compartment as well as extracellularly, experiments were performed at two pH values, i.e. pH 5.5 to simulate endolysosomal conditions and pH 7.4 to mimic extracellular conditions. Optimal incubation periods for the cleavage reactions were determined to be 30 min at pH 5.5 and 15 min at pH 7.4 (data not shown). The mixtures of cleavage products were analyzed by MALDI-TOF mass spectrometry to identify the cleavage sites within

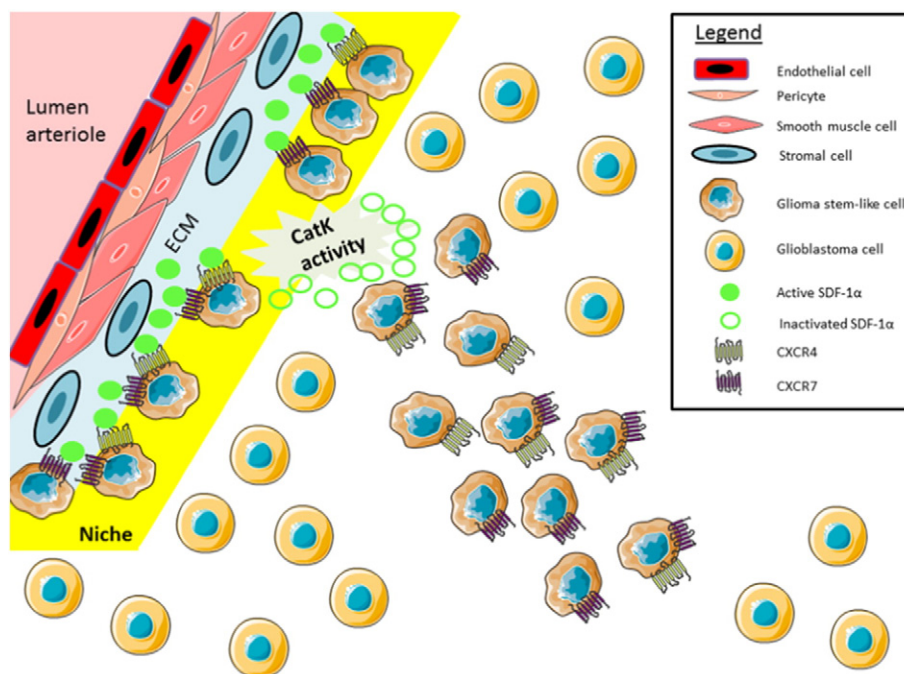


Fig. 5. Schematic representation of the GSLC niche. Our proposed model of GSLC niches around arterioles. The arteriolar wall consists of an endothelial cell layer surrounded by pericytes and smooth muscle cells and the adventitia (stroma) containing ECM and stromal cells. Endothelial cells and/or GBM cells secrete proteases, including CatK, that cleave SDF-1 α in GSLC niches and loosen anchorage of GSLCs that express CXCR4 and/or CXCR7. CatK cleavage of SDF-1 α enables mobilization of GSLCs out of niches.

SDF-1 α . In both conditions, peaks with average molecular masses of 7964.375, 7552.878 and 7352.643 Da, respectively, were identified. These correspond to the singly protonated forms (MH⁺) of full-length SDF-1 α , and two N-terminally-cleaved fragments, the larger being cleaved after Ser4 and the smaller after Ser6. Two additional fragments were observed at pH 7.4 with molecular masses of 6729.879 and 4582.347 Da, respectively. These correspond to SDF-1 α fragments produced by cleavage after Cys11 and Leu29. The kinetics of the reaction

showed that larger numbers of fragments appeared after shorter incubation periods at pH 7.4 than at pH 5.5 (Fig. 2), indicating that CatK cleaves SDF-1 α more readily at physiological extracellular pH. The positions of the cleavage sites in the three-dimensional (3D) structure of SDF-1 α are shown in Fig. 2B. Chemokines are known to interact with two sites on their receptors, where the globular part of the chemokine interacts with the N-terminal extension of the receptor, and the N-terminus of the chemokine binds to the functional site of the receptor

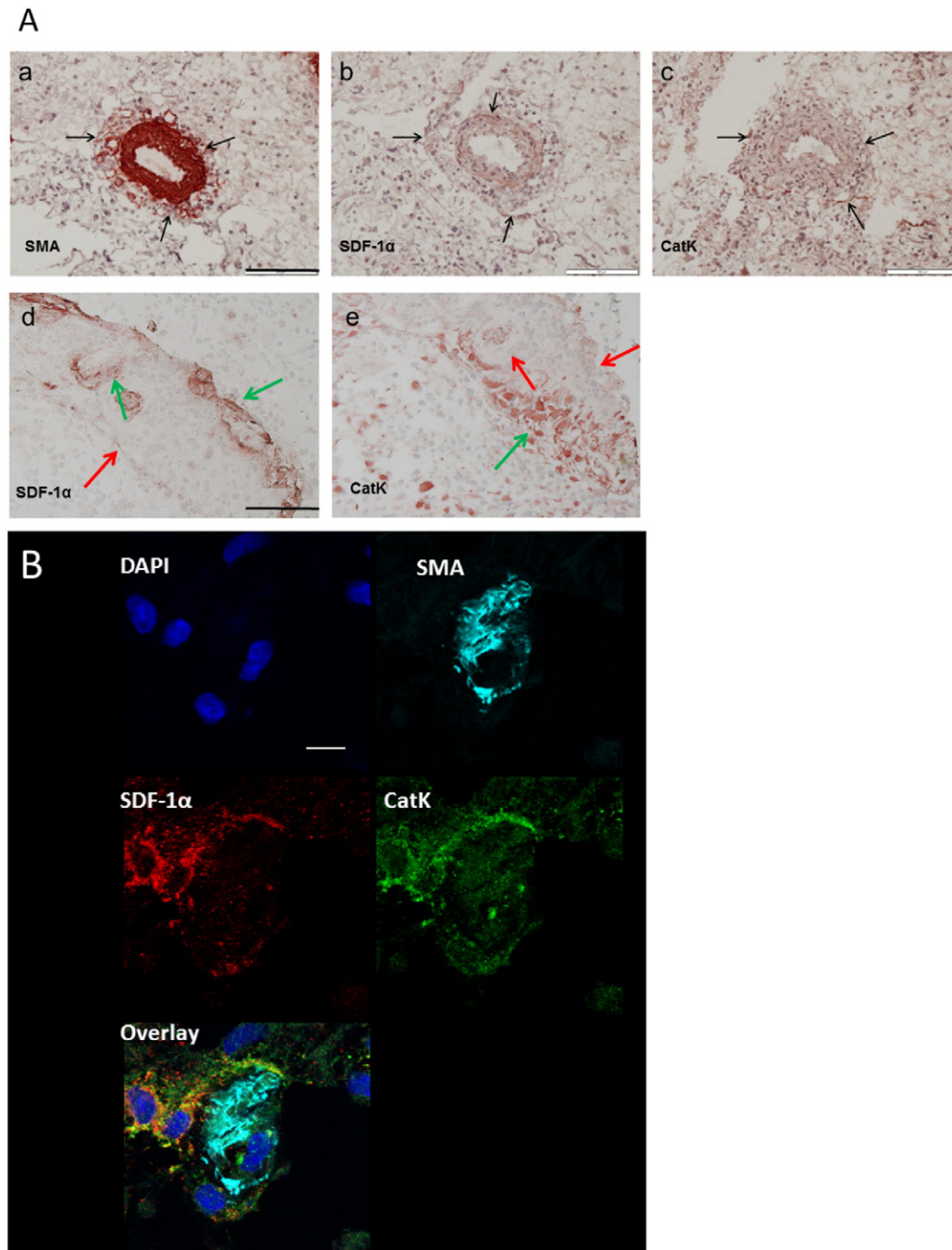


Fig. 6. Immunolocalization of SDF-1 α and CatK in niches around arterioles. (A) Immunohistochemical staining of SMA (a), SDF-1 α (b) and CatK (c) was performed on human serial cryostat sections of GBM, showing the expression of SDF-1 α and CatK in GSCL niches around SMA-positive arterioles and in the arteriolar wall (indicated by black arrows). SMA stains smooth muscle cells of the arteriolar wall, which is the center of GSCL niches. (d, e) Inverse correlation of SDF-1 α and CatK protein expression in niches in serial cryostat sections of GBM. Red arrows indicate low protein expression and green arrows indicate higher protein expression. Sections were counterstained with hematoxylin to detect nuclei. Scale bar = 100 μ m. (B) Fluorescence immunohistochemical staining of SMA, SDF-1 α and CatK was performed on human serial cryostat sections of GBM and imaging by confocal microscopy showed co-localization of SDF-1 α (red) and CatK (green) around SMA-positive arterioles (light blue). SDF-1 α and CatK were partly co-localized (yellow). Sections were counterstained with DAPI to detect the nuclei. Scale bar = 10 μ m.

[40,41]. The N-terminal cleavage sites of CatK are located in the flexible region of SDF-1 α that is responsible for binding to the functional site of CXCR4/CXCR7 and for triggering of signaling. It has been shown that cleavage of 2 residues from the N-terminus is sufficient to abolish activation of the receptor [42]. The remaining 2 cleavage sites are located in the globular part of the molecule at positions that are directly involved in the interactions with the N-terminal part of CXCR4/CXCR7 [43]. It is thus likely that CatK cleavage prevents SDF-1 α from binding to CXCR4/CXCR7. To test whether SDF-1 α cleavage by CatK inhibits chemotaxis, transwell invasion assays were performed using either SDF-1 α as a chemo-attractant or the CatK-induced cleavage products of SDF-1 α (Section 3.3).

3.3. CatK cleavage of SDF-1 α prevents transwell invasion

Transwell invasion assays were performed with NCH421k and U87 cells to determine the chemotactic activity of SDF-1 α and its cleavage products and PepC-C. The relative invasion of U87 and NCH421k cells was higher in the presence of SDF-1 α and PepC-C than in the presence of reaction mixtures, SDF-1 α cleavage products, synthetic SDF-1 α N-terminal peptides or control conditions and this effect was significant (Fig. 3). Fig. 3 shows significant chemotactic effects of SDF-1 α and PepC-C on NCH421k and U87 cells as compared to the control. There was no significant difference between the effects of SDF-1 α and PepC-C (Fig. 3). Cleavage products of SDF-1 α generated by CatK at pH 5.5 and 7.4, both in the complete reaction mixtures and after filtration to remove peptides larger than 3 kDa, did not show any chemotactic effects. The filtration step was performed to specifically determine the effects of SDF-1 α -derived small peptides from the N-terminus (Fig. 2). These data indicate that SDF-1 α cleavage by CatK at both pH 5.5 and 7.4 completely abolished the chemotactic effects of SDF-1 α . To study these phenomena further, 2 small peptides from the N-terminus of SDF-1 α were synthesized and tested in transwell invasion assays. Fig. 3 shows that these synthetic peptides had no chemotactic effects either alone or together. Since we did not observe any difference between the effects of complete reaction mixtures and filtrated small cleavage products, all further

experiments were performed with the filtrated small cleavage products only.

3.4. CatK cleavage of SDF-1 α prevents Matrigel invasion from spheroids

Invasion assays were performed in 3D to study the invasive behaviour of NCH421k cells that were growing as spheroids in Matrigel (Fig. 4A). Treatment of the spheroids with SDF-1 α and PepC-C resulted in a significantly increased number of NCH421k cells that invaded Matrigel out of the spheroids, as compared to the control (Fig. 4Aa–c). CatK-induced cleavage products of SDF-1 α at pH 5.5 and 7.4 did not stimulate invasion of GSLCs out of the spheroids as the invasion was similar to that in control conditions (Fig. 4Aa, d, e). This invasive pattern was observed both after 3 and 6 days.

3.5. Schematic representation of the GSLC niche

Fig. 5 shows our concept of the GSLC niche. CXCR4 and/or CXCR7-expressing GSLCs are retained around arterioles in the GSLC niche by SDF-1 α /CXCR4 and/or SDF-1 α /CXCR7 interactions as was found in our previous study [9]. The arteriolar wall consists of endothelial cells, pericytes, smooth muscle cells and the adventitia which consists of stroma containing extracellular matrix (ECM) and stromal cells. The GSLCs are attached to the stroma via SDF-1 α /CXCR4/7 interactions. CatK activity induces cleavage and inactivation of SDF-1 α , which results in migration of GSLCs out of GSLC niches.

3.6. SDF-1 α and CatK expression around arterioles in GSLC niches

Chromogenic and fluorescence IHC were performed to provide supporting evidence for our concept of the GSLC niche as illustrated in Fig. 5. Human GBM serial cryostat sections were used for chromogenic IHC to localize SDF-1 α and CatK in GSLC niches. Fig. 6Aa–c shows that SDF-1 α and CatK are both localized around SMA-positive arterioles of GSLC niches and are also expressed in the arteriolar wall. SDF-1 α and CatK were expressed around arterioles. In addition, we found SDF-1 α and CatK expression in an inverse correlation in niches (Fig. 6Ad, e).

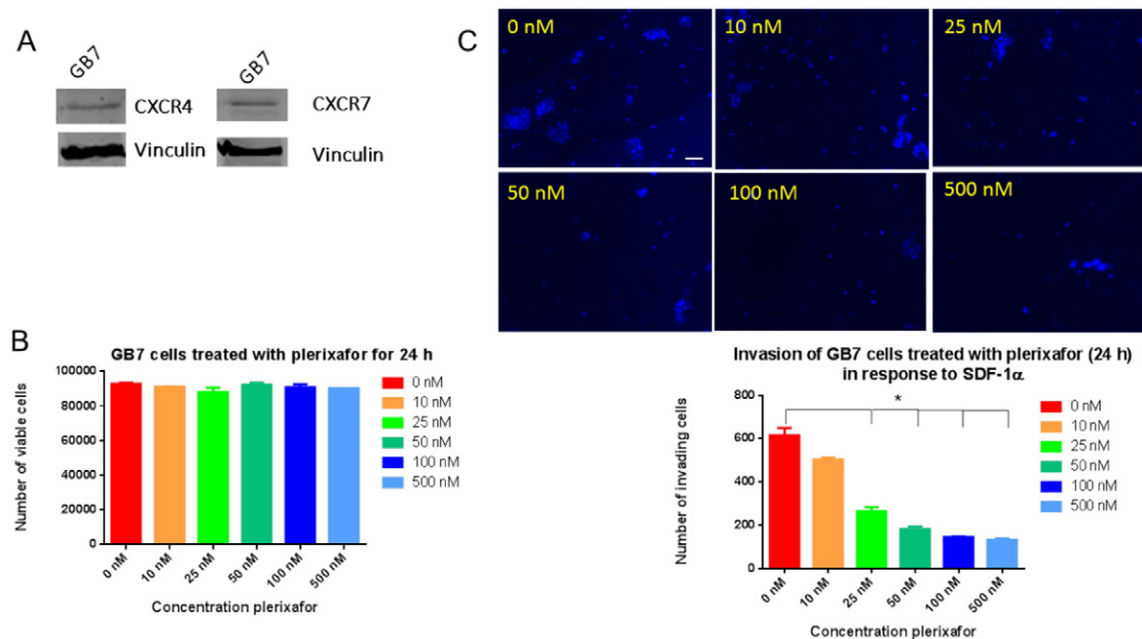


Fig. 7. CXCR4 inhibitor plerixafor inhibits invasion of CXCR4/CXCR7-expressing GB7 GSLCs. (A) Western blot data shows that GB7 GSLCs express both CXCR4 and CXCR7. Vinculin is used as loading control. (B) Cell viability assays were performed to determine toxicity of plerixafor. Treatment with 10, 25, 50, 100 and 500 nM plerixafor for 24 h did not affect cell viability. (C) Transwell invasion assays were performed with GB7 GSLCs treated with 10, 25, 50, 100 and 500 nM plerixafor for 24 h with SDF-1 α in the lower chamber as chemoattractant. The data shows that plerixafor reduces the number of invading cells significantly. DAPI-stained cells were counted using ImageJ software. Scale bar = 50 μ m. The error bars represent the standard error of the mean. *, $P < 0.05$.

Fluorescence IHC and confocal imaging of human GBM cryostat sections showed that SDF-1 α and CatK are co-localized around SMA-positive arterioles of GSLC niches (Fig. 6B).

3.7. CXCR4 inhibitor plerixafor inhibits invasion of GSLCs

Since our data provides supporting evidence that the SDF-1 α /CXCR4/CXCR7 axis is involved in retaining CXCR4/CXCR7-expressing GSLCs in SDF-1 α -containing niches, we determined the effect of the CXCR4 inhibitor plerixafor on invasion of GSLCs in response to SDF-1 α . Western blot analysis revealed that GB7 GSLCs express both CXCR4 and CXCR7. Vinculin was used as loading control (Fig. 7A). Next, we determined the toxicity of plerixafor by performing cell viability assays. The data shows that treatment with plerixafor does not affect cell viability after 24 h (Fig. 7B), confirming that plerixafor is not toxic for the cells. Transwell invasion assays were performed to determine the effect of plerixafor on invasion of GB7 GSLCs, which were treated with various concentrations of plerixafor for 24 h and SDF-1 α was used as chemo-attractant. Fig. 7C shows a concentration-dependent effect of plerixafor with a significant reduction in the number of invading GB7 GSLCs as compared to the control and 500 nM plerixafor had the highest inhibitory effect on invasion.

4. Discussion

The present study shows that SDF-1 α induces chemotactic responses of U87 GBM cells, and NCH421k and GB7 GSLCs supporting the concept that SDF-1 α recruits GSLCs to the wall of arterioles, where GSLC niches are located. Our qRT-PCR data revealed that U87 cells have higher levels of SDF-1 α receptor CXCR4 mRNA, whereas the NCH421k cells have higher levels of CXCR7 mRNA. However, the flow cytometry analysis showed that both U87 and NCH421k cells express high levels of CXCR4 protein and lower CXCR7 protein levels at their surface. We assume that either CXCR7 protein in NCH421k cells is mainly present intracellularly in granules or that turnover rates of the receptors in the 2 cell lines are different. In addition, our western blot analysis showed that the GB7 cells express both CXCR4 and CXCR7 in serum-free conditions. Hattermann et al. in 2010 found in serum-containing media that CXCR4 was expressed in GSLCs and differentiated GBM cells whereas CXCR7 was expressed in differentiated GBM cells [45]. Our data is in line with other studies that showed that CXCR4 and CXCR7 are essential for functioning of brain tumor cells [18–21]. U87 and NCH421k cells differ in the expression of CXCR7, but we found similar chemotactic responses *in vitro* towards SDF-1 α (Fig. 3). GB7 GSLCs also express both CXCR4 and CXCR7 (Fig. 7A) and these cells are strongly attracted towards SDF-1 α (Fig. 7C). This chemoattraction was inhibited by the CXCR4 inhibitor plerixafor (Fig. 7C) which was also shown recently by Yadev et al. in their study of perivascular invasion of GBM cells and GSLCs [46], which is in line with our concept that the SDF-1 α /CXCR4 axis is involved in retaining CXCR4-expressing GSLCs in SDF-1 α -containing niches (Fig. 5). We have not tested the CXCR7-inhibitor CX662 in our GSLC models. It is likely that CXCR7 is less involved in the process of invasion than CXCR4, since the SDF-1 α /CXCR7 axis activates β -arrestin, resulting in scavenging of SDF-1 α . The heterodimeric SDF-1 α /CXCR4/CXCR7 signaling axis induces a conformational change of CXCR4 and G-proteins and blocks further signaling [18]. Since CatK activation is a complicated and highly regulated process, CXCR4/CXCR7 inhibition may be a more promising strategy to enforce GSLCs out of their niches than activation of CatK.

Protease signaling via modifications of their substrates may affect cytokine activity which is a complex feedback loop between the families of proteases and cytokines [47]. The co-localization and inverse correlation between expression of SDF-1 α and CatK proteins in GSLC niches (Fig. 6) suggests that extralysosomal CatK cleaves and inactivates SDF-1 α , with the consequence of the release of GSLCs from niches (Fig. 5). Extracellular SDF-1 α can be explained by secretion by endothelial

cells and stromal cells and is upregulated by HIF-1 α and VEGF [17]. SDF-1 α can be present intracellularly as well as it can be internalized after binding to CXCR7 [18]. CatK is an endolysosomal protease and is therefore present intracellularly, but can also be present extracellularly when secreted by GBM cells or endothelial cells.

CatK was found to be one of the highest differentially expressed proteases in GBM tissues and cells versus their normal counterparts [29], but we have not been able to show its activity in GBM tissue and cell lysates. This suggests that CatK activity is *in vivo* highly regulated by proteolytic, possibly autolytic activation of its precursor form [39], which may depend on pH and redox potential which in turn are regulated by glutathione and hydrogen peroxide. The latter inhibits the processing of the proenzyme and inactivates mature CatK [48]. CatK has already been reported as one of the proteases besides MMP-2, MMP-9, neutrophil elastase and cathepsin G, that can inactivate SDF-1 α by cleaving off amino acids from the N-terminus of SDF-1 α [49]. Later, Staudt et al. showed that all 11 constitutively secreted cysteine cathepsins can cleave SDF-1 α to modulate the communication between HSCs and their niches in the bone marrow, and all were secreted as proteolytically inactive enzymes [39]. Most cleavages of SDF-1 α were observed with CatB that is highly expressed in GBM [30,31], and, therefore, a possible cooperation between CatK and CatB in regulating chemotactic activity of SDF-1 α *in vivo* cannot be excluded.

The N-terminal domain of SDF-1 α which binds with residues 12–17 (RFFESH) to CXCR4 acts as an initial docking site for SDF-1 α . After binding, the activation domain composed of amino acid residues 1–8 (KPVLSYR) binds to the N-terminal end of the receptor, inducing a conformational change that allows binding of G-proteins to the intracellular domain of the receptor, leading to activation of signaling pathways described above [18]. Filipo et al. (2013) demonstrated that the N-terminal sequence of SDF-1 α , PepC-C (KPVLSYRCPFFESHARA), is sufficient to stimulate proliferation and chemotaxis of neural stem cells from the subventricular zone to injury sites in the cortex, thus possessing full SDF-1 α activity [36]. Here, we demonstrated that CatK cleaves SDF-1 α at 3 positions beyond the amino acid 21 position of N-terminal PepC-C, thus completely inactivating SDF-1 α activity. The two small synthetic peptides of the N-terminus of SDF-1 α (KPVV and KPVVLS) did not show chemotactic activity, retaining U87 and NCH421k cell invasion at control levels (Fig. 3). In contrast, PepC-C was chemotactically active in a similar way as intact SDF-1 α in invasion assays, as was shown previously [36]. It would be interesting to determine whether treatment with the two small peptides together with SDF-1 α results in inhibition of the chemotactic activity of SDF-1 α , as the two small peptides may be able to bind to the active site of CXCR4/7 receptors without activating them and preventing the SDF-1 α binding. The bulk of the SDF-1 α protein is not involved in the chemotactic activity (Fig. 2). Therefore, it may have a function in protection of the active N-terminus of SDF-1 α against degradation.

In conclusion, the present study provides supporting evidence for our concept of the GSLC niche that CatK activity releases GSLCs from niches by inactivating SDF-1 α and we proposed the novel therapeutic approach that disrupts SDF-1 α /CXCR4 and/or SDF-1 α /CXCR7 interactions to enhance GSLC migration out of niches, with subsequent loss of their stemness and sensitization to chemo-irradiation. Therefore, it is relevant to study CatK activity in more detail. An interesting question that arises is whether CatK should be inhibited, as has been suggested for many types of cancer [28], or rather upregulated. In line with this up-regulation, Lopez-Otin et al. in 2007 reported that the activity of many proteases in cancer have tumor suppressing effects rather than tumorigenic effects [50]. We therefore suggest that CatK activity should be up-regulated in GBM before and during chemo-irradiation, since this may sensitize GSLCs to chemo-irradiation.

Transparency document

The [Transparency document](#) associated with this article can be found, in online version.

Acknowledgements

This study was supported by a René Vogels travel grant (VVVH), a JoKolk scholarship (VVVH), the Dutch Cancer Society grant (KWF; UVA 2014–6839; VVVH, CJFVN), the Slovenian Research Agency (ARRS) Programme Grants (P1-0245 and P1-0140; TTL, MN) and ARRS Young Researchers Grant (UV, BB), and by the Fundação de Amparo à Pesquisa do Estado de São Paulo (FAPESP-12/50191-AR).

References

- R. Kalkan, Glioblastoma stem cells as a new therapeutic target for glioblastoma, *Clin. Med. Insights Oncol.* 9 (2015) 95–103.
- D. Schiffer, M. Mellai, L. Annovazzi, V. Caldera, A. Piazzi, T. Denysenko, A. Melcarne, Stem cell niches in glioblastoma: a neuropathological view, *Biomed. Res. Int.* 2014 (2014) 725921.
- S.E. Mir, P.C. De Witt Hamer, P.M. Krawczyk, L. Balaj, A. Claes, J.M. Niers, A.A. Van Tilborg, A.H. Zwinderman, D. Geerts, G.J. Kaspers, W. Peter Vandertop, J. Cloos, B.A. Tannous, P. Wesseling, J.A. Aten, D.P. Noske, C.J. Van Noorden, T. Wurdinger, In silico analysis of kinase expression identifies WEE1 as a gatekeeper against mitotic catastrophe in glioblastoma, *Cancer Cell* 18 (2010) 244–257.
- A.R. Rama, P.J. Alvarez, R. Madeddu, A. Aranega, ABC transporters as differentiation markers in glioblastoma cells, *Mol. Biol. Rep.* 41 (2014) 4847–4851.
- J.D. Lathia, M. Li, P.E. Hall, J. Gallagher, J.S. Hale, Q. Wu, M. Venere, E. Levy, M.R. Rani, P. Huang, E. Bae, J. Selfridge, L. Cheng, H. Guvenc, R.E. McLendon, I. Nakano, A.E. Sloan, H.S. Phillips, A. Lai, C.L. Gladson, M. Bredel, S. Bao, A.B. Hjelmeland, J.N. Rich, Laminin alpha 2 enables glioblastoma stem cell growth, *Ann. Neurol.* 72 (2012) 766–778.
- A.B. Hjelmeland, Q. Wu, S. Wickman, C. Eyler, J. Hedderston, Q. Shi, J.D. Lathia, J. Macsworlds, J. Lee, R.E. McLendon, J.N. Rich, Targeting A20 decreases glioma stem cell survival and tumor growth, *PLoS Biol.* 8 (2010) e1000319.
- P.J. Richardson, CXCR4 and glioblastoma, *Anticancer Agents Med Chem.* 16 (2015) 59–74.
- D. Hambardzumyan, G. Bergers, Glioblastoma: defining tumor niches, *Trends Cancer* 1 (2015) 252–265.
- V.V. Hira, K.J. Ploegmakers, F. Grevers, U. Verbovsek, C. Silvestre-Roig, E. Aronica, W. Tigchelaar, T.L. Turnsek, R.J. Molenaar, C.J. Van Noorden, CD133⁺ and Nestin⁺ glioma stem-like cells reside around CD31⁺ arterioles in niches that express SDF-1alpha, CXCR4, osteopontin and cathepsin K, *J. Histochem. Cytochem.* 63 (2015) 481–493.
- P.E. Boulais, P.S. Frenette, Making sense of hematopoietic stem cell niches, *Blood* 125 (2015) 2621–2629.
- A. Ehninger, A. Trumpff, The bone marrow stem cell niche grows up: mesenchymal stem cells and macrophages move in, *J. Exp. Med.* 208 (2011) 421–428.
- O. Kollet, A. Dar, S. Shvitiel, A. Kalinkovich, K. Lapid, Y. Sztainberg, M. Tesio, R.M. Samstein, P. Goichberg, A. Spiegel, A. Elson, T. Lapidot, Osteoclasts degrade endosteal components and promote mobilization of hematopoietic progenitor cells, *Nat. Med.* 12 (2006) 657–664.
- S.J. Morrison, D.T. Scadden, The bone marrow niche for haematopoietic stem cells, *Nature* 505 (2014) 327–334.
- A.D. Lander, J. Kimble, H. Clevers, E. Fuchs, D. Montarras, M. Buckingham, A.L. Calof, A. Trumpff, T. Oskarsson, What does the concept of the stem cell niche really mean today? *BMC Biol.* 10 (2012) 19.
- B. Joddar, Y. Ito, Artificial niche substrates for embryonic and induced pluripotent stem cell cultures, *J. Biotechnol.* 168 (2013) 218–228.
- D. Zagzag, M. Esencay, O. Mendez, H. Yee, I. Smirnova, Y. Huang, L. Chiriboga, E. Lukyanov, M. Liu, E.W. Newcomb, Hypoxia- and vascular endothelial growth factor-induced stromal cell-derived factor-1alpha/CXCR4 expression in glioblastomas: one plausible explanation of Scherer's structures, *Am. J. Pathol.* 173 (2008) 545–560.
- D. Zagzag, Y. Lukyanov, L. Lan, M.A. Ali, M. Esencay, O. Mendez, H. Yee, E.B. Voura, E.W. Newcomb, Hypoxia-inducible factor 1 and VEGF upregulate CXCR4 in glioblastoma: implications for angiogenesis and glioma cell invasion, *Lab. Invest.* 86 (2006) 1221–1232.
- R. Wurth, A. Bajetto, J.K. Harrison, F. Barbieri, T. Florio, CXCL12 modulation of CXCR4 and CXCR7 activity in human glioblastoma stem-like cells and regulation of the tumor microenvironment, *Front. Cell. Neurosci.* 8 (2014) 144.
- R. Sengupta, A. Dubuc, S. Ward, L. Yang, P. Northcott, B.M. Woerner, K. Kroll, J. Luo, M.D. Taylor, R.J. Wechsler-Reya, J.B. Rubin, CXCR4 activation defines a new subgroup of Sonic hedgehog-driven medulloblastoma, *Cancer Res.* 72 (2012) 122–132.
- M.J. Walters, K. Ebsworth, R.D. Berahovich, M.E. Penfold, S.C. Liu, R. Al Omran, M. Kioi, S.B. Chernikova, D. Tseng, E.E. Mulkearns-Hubert, M. Sinyuk, R.M. Ransohoff, J.D. Lathia, J. Karamchandani, H.E. Kohrt, P. Zhang, J.P. Powers, J.C. Jaen, T.J. Schall, M. Merchant, L. Recht, J.M. Brown, Inhibition of CXCR7 extends survival following irradiation of brain tumours in mice and rats, *Br. J. Cancer* 110 (2014) 1179–1188.
- J.B. Rubin, A.L. Kung, R.S. Klein, J.A. Chan, Y. Sun, K. Schmidt, M.W. Kieran, A.D. Luster, R.A. Segal, A small-molecule antagonist of CXCR4 inhibits intracranial growth of primary brain tumors, *Proc. Natl. Acad. Sci. U. S. A.* 100 (2003) 13513–13518.
- D.G. Duda, S.V. Kozin, N.D. Kirkpatrick, L. Xu, D. Fukumura, R.K. Jain, CXCL12 (SDF1alpha)-CXCR4/CXCR7 pathway inhibition: an emerging sensitizer for anticancer therapies? *Clin. Cancer Res.* 17 (2011) 2074–2080.
- S. Kenig, M.B. Alonso, M.M. Mueller, T.T. Lah, Glioblastoma and endothelial cells cross-talk, mediated by SDF-1, enhances tumour invasion and endothelial proliferation by increasing expression of cathepsins B, S, and MMP-9, *Cancer Lett.* 289 (2010) 53–61.
- C.C. Bleul, R.C. Fuhlbrigge, J.M. Casasnovas, A. Aiuti, T.A. Springer, A highly efficacious lymphocyte chemoattractant, stromal cell-derived factor 1 (SDF-1), *J. Exp. Med.* 184 (1996) 1101–1109.
- Y. Uemae, E. Ishikawa, S. Osuka, M. Matsuda, N. Sakamoto, S. Takano, K. Nakai, T. Yamamoto, A. Matsumura, CXCL12 secreted from glioma stem cells regulates their proliferation, *J. Neurooncol* 117 (2014) 43–51.
- M. Terasaki, Y. Sugita, F. Arakawa, Y. Okada, K. Ohshima, M. Shigemori, CXCL12/CXCR4 signaling in malignant brain tumors: a potential pharmacological therapeutic target, *Brain Tumor Pathol.* 28 (2011) 89–97.
- I. Kryczek, S. Wei, E. Keller, R. Liu, W. Zou, Stroma-derived factor (SDF-1/CXCL12) and human tumor pathogenesis, *Am. J. Physiol. Cell Physiol.* 292 (2007) C987–C995.
- U. Verbovsek, C.J. Van Noorden, T.T. Lah, Complexity of cancer protease biology: cathepsin K expression and function in cancer progression, *Semin. Cancer Biol.* 35 (2015) 71–84.
- U. Verbovsek, H. Motaln, A. Rotter, N.A. Atai, K. Gruden, C.J. Van Noorden, T.T. Lah, Expression analysis of all protease genes reveals cathepsin K to be overexpressed in glioblastoma, *PLoS One* 9 (2014) e111819.
- B. Gole, P.C. Huszthy, M. Popovic, J. Jeruc, Y.S. Ardebili, R. Bjerkvig, T.T. Lah, The regulation of cysteine cathepsins and cystatins in human gliomas, *Int. J. Cancer* 131 (2012) 1779–1789.
- T.T. Lah, M.B. Duran Alonso, C.J. Van Noorden, Antiprotease therapy in cancer: hot or not? *Expert Opin. Biol. Ther.* 6 (2006) 257–279.
- N. Podergajs, H. Motaln, U. Rajcevic, U. Verbovsek, M. Korsic, N. Obad, H. Espedal, M. Vittori, C. Herold-Mende, H. Miletic, R. Bjerkvig, T.L. Turnsek, Transmembrane protein CD9 is glioblastoma biomarker, relevant for maintenance of glioblastoma stem cells, *Oncotarget* 7 (2016) 593–609.
- K. Kolosa, H. Motaln, C. Herold-Mende, M. Korsic, T.T. Lah, Paracrine effects of mesenchymal stem cells induce senescence and differentiation of glioblastoma stem-like cells, *Cell Transplant.* 24 (2015) 631–644.
- A. Torsvik, G.V. Rosland, A. Svendsen, A. Molven, H. Immervoll, E. McCormack, P.E. Lonning, M. Primon, E. Sobala, J.C. Tonn, R. Goldbrunner, C. Schichor, J. Mysliwicz, T.T. Lah, H. Motaln, S. Knappskog, R. Bjerkvig, Spontaneous malignant transformation of human mesenchymal stem cells reflects cross-contamination: putting the research field on track – letter, *Cancer Res.* 70 (2010) 6393–6396.
- M. Novinec, M. Pavsic, B. Lenarcic, A simple and efficient protocol for the production of recombinant cathepsin V and other cysteine cathepsins in soluble form in *Escherichia coli*, *Protein Expr. Purif.* 82 (2012) 1–5.
- T.R. Filippo, L.T. Galindo, G.F. Barnabe, C.B. Ariza, L.E. Mello, M.A. Juliano, M.A. Porcionatto, CXCL12 N-terminal end is sufficient to induce chemotaxis and proliferation of neural stem/progenitor cells, *Stem Cell Res.* 11 (2013) 913–925.
- P. Chieco, A. Jonker, B.A. De Boer, J.M. Ruijter, C.J. Van Noorden, Image cytometry: protocols for 2D and 3D quantification in microscopic images, *Prog. Histochem. Cytochem.* 47 (2013) 211–333.
- C.A. Schneider, W.S. Rasband, K.W. Eliceiri, NIH Image to ImageJ: 25 years of image analysis, *Nat. Methods* 9 (2012) 671–675.
- N.D. Staudt, A. Maurer, B. Spring, H. Kalbacher, W.K. Aicher, G. Klein, Processing of CXCL12 by different osteoblast-secreted cathepsins, *Stem Cells Dev.* 21 (2012) 1924–1935.
- J.E. Pease, J. Wang, P.D. Ponath, P.M. Murphy, The N-terminal extracellular segments of the chemokine receptors CCR1 and CCR3 are determinants for MIP-1alpha and eotaxin binding, respectively, but a second domain is essential for efficient receptor activation, *J. Biol. Chem.* 273 (1998) 19972–19976.
- F.S. Monteclaro, I.F. Charo, The amino-terminal domain of CCR2 is both necessary and sufficient for high affinity binding of monocyte chemoattractant protein 1. Receptor activation by a pseudo-tethered ligand, *J. Biol. Chem.* 272 (1997) 23186–23190.
- M.P. Crump, J.H. Gong, P. Loetscher, K. Rajarathnam, A. Amara, F. Arenzana-Seisdedos, J.L. Virelizier, M. Baggiolini, B.D. Sykes, I. Clark-Lewis, Solution structure and basis for functional activity of stromal cell-derived factor-1; dissociation of CXCR4 activation from binding and inhibition of HIV-1, *EMBO J.* 16 (1997) 6996–7007.
- J.J. Ziarek, A.E. Getschman, S.J. Butler, D. Taleski, B. Stephens, I. Kufareva, T.M. Handel, R.J. Payne, B.F. Volkman, Sulfoxide probes of the CXCR4/CXCL12 interface reveal oligomer-specific contacts and chemokine allostery, *ACS Chem. Biol.* 8 (2013) 1955–1963.
- E.F. Pettersen, T.D. Goddard, C.C. Huang, G.S. Couch, D.M. Greenblatt, E.C. Meng, T.E. Ferrin, UCSF chimera—a visualization system for exploratory research and analysis, *J. Comput. Chem.* 25 (2004) 1605–1612.
- K. Hattermann, J. Held-Feindt, R. Lucius, S.S. Muerkoster, M.E. Penfold, T.J. Schall, R. Mentlein, The chemokine receptor CXCR7 is highly expressed in human glioma cells and mediates antiapoptotic effects, *Cancer Res.* 70 (2010) 3299–3308.
- V.N. Yadav, D. Zamlar, G.J. Baker, P. Kadiyala, A. Erdreich-Epstein, A.C. DeCarvalho, T. Mikkelsen, M.G. Castro, P.R. Lowenstein, CXCR4 increases in-vivo glioma perivascular invasion, and reduces radiation induced apoptosis: a genetic knock-down study, *Oncotarget* 7 (2016) 83701–83719.
- B. Turk, D. Turk, V. Turk, Protease signalling: the cutting edge, *EMBO J.* 31 (2012) 1630–1643.
- M. Novinec, B. Lenarcic, A. Baici, Probing the activity modification space of the cysteine peptidase cathepsin K with novel allosteric modifiers, *PLoS One* 9 (2014) e106642.
- S.Y. Cho, M. Xu, J. Roboz, M. Lu, J. Mascarenhas, R. Hoffman, The effect of CXCL12 processing on CD34⁺ cell migration in myeloproliferative neoplasms, *Cancer Res.* 70 (2010) 3402–3410.
- C. Lopez-Otin, L.M. Matrisian, Emerging roles of proteases in tumour suppression, *Nat. Rev. Cancer* 7 (2007) 800–808.